

## Aviation Applications for Satellite-based Observations of Cloud Properties, Convection Initiation, In-flight Icing, Turbulence and Volcanic Ash

John R. Mecikalski<sup>#</sup>

Wayne F. Feltz<sup>\*</sup>

John J. Murray<sup>§</sup>

David B. Johnson<sup>Ø</sup>

Kristopher M. Bedka<sup>\*</sup>

Sarah M. Bedka<sup>\*</sup>

Anthony J. Wimmers<sup>\*</sup>

Michael Pavolonis <sup>^</sup>

Todd A. Berendes<sup>#</sup>

Julie Haggerty<sup>Ø</sup>

Pat Minnis<sup>§</sup>

Ben Bernstein<sup>Ø</sup>

Earl Williams<sup>&</sup>

For publication in *Bulletin of the American Meteorological Society*

<sup>#</sup>Atmospheric Science Department, University of Alabama in Huntsville

<sup>\*</sup>Cooperative Institute for Meteorological Satellite Studies, University of Wisconsin–Madison

<sup>§</sup>NASA Langley Research Center, Chemistry and Dynamics Branch, Hampton, Virginia

<sup>Ø</sup>NCAR, Research Applications Program, Boulder, Colorado

<sup>^</sup>NOAA/NESDIS Advanced Satellite Products Branch, Madison, Wisconsin

<sup>&</sup> Massachusetts Institute of Technology, Lincoln Laboratory

## Abstract

Advanced Satellite Aviation Weather Products (ASAP) was jointly initiated by the NASA Applied Sciences Program and the NASA Aviation Safety and Security Program in 2002. The initiative provides a valuable bridge for transitioning new and existing satellite information and products into Federal Aviation Administration (FAA) Aviation Weather Research Program (AWRP) efforts to increase the safety and efficiency of the airspace system. The ASAP project addresses hazards such as convective weather, turbulence (clear-air and cloud-induced), icing and volcanic ash and is particularly applicable in extending the monitoring of weather over data-sparse areas such as the oceans and other observationally remote locations.

ASAP research is conducted by scientists from NASA, the FAA AWRP's Product Development Teams (PDT), NOAA and the academic research community. In this paper we provide a summary of activities since the inception of ASAP that emphasize the use of current-generation satellite technologies toward observing and mitigating specified aviation hazards. A brief overview of future ASAP goals is also provided in light of the next generation of satellite sensors (e.g., hyperspectral; high spatial resolution) to become operational in the 2006-2013 timeframe.

## 1) Introduction

Weather hazards can reduce the safety and constrain the efficiency of our national air navigation system. Not only are most of the air traffic delays caused by weather, but weather is also a factor in many fatal accidents. The Federal Aviation Administration's National Aviation Safety Data Analysis Center (NASDAC), in a study of the National Transportation Safety Board (NTSB) accident database<sup>1</sup>, discovered that between 1991 and 2001, there were 22,655 aircraft accidents involving 22,973 aircraft. Weather was a contributing or causal factor in 4,771 (21.1%) of these accidents. In particular, wind and ceiling/visibility contributed to over 90% of this total. Other factors (comprising the remaining 10%) include turbulence and density altitude, with turbulence alone estimated to cost the airline industry about \$750 million per year (Triplett 2005). NTSB data indicate 41.4% of all weather-related accidents show no record of weather briefing. From 1991 to 2001, the annual number of weather-related accidents has declined. However, the annual number of weather-related accidents has remained roughly constant as a percentage of total accidents.

From the earliest days of aviation it was clear that high quality weather observations and accurate weather forecasts were critical to the safe operation of aircraft. In the early 20<sup>th</sup> Century the development of a national meteorological surface observing system paralleled the expansion of the aviation industry. After World War II weather radars gradually came into widespread use for detecting the location, height, and movement of major storm systems for general public safety and support of aviation. In the 1980s the National Weather Service (NWS) began a nationwide modernization program, in partnership with the Federal Aviation Administration

---

<sup>1</sup> A summary of the study's conclusions is available at [www.nasdac.faa.gov/aviation\\_studies/weather\\_study/summary.html](http://www.nasdac.faa.gov/aviation_studies/weather_study/summary.html) or from the Office of Systems Safety, Federal Aviation Administration, 800 Independence Avenue, SW, Washington, DC 20591.

(FAA), to upgrade weather-observing systems including next generation weather radars (Weather Surveillance Radars 1988 Doppler—WSR88D) and automated surface observing systems (National Research Council 1980; 1991; 1994).

The movement toward specialized meteorological observing systems to support aviation was accelerated by Ted Fujita's identification of small-scale wind patterns from convective storms that caused a number of major airline crashes (Fujita 1985; 1986). The need for operational detection of these wind patterns led the FAA to install specially designed Terminal Doppler Weather Radars (TDWR) or Low Level Windshear Alert Systems (LLWAS) at many of the major airports in the United States. The parallel need for high-resolution, rapidly updated aviation weather forecasts led to the development of special numerical weather prediction models, such as the National Centers for Environmental Prediction's (NCEP) Rapid Update Cycle Model (RUC).

During this same time period, satellite-observing systems were also undergoing a rapid expansion in their capabilities and availability and represented an underutilized resource for enhancing aviation weather products. Recognizing that advanced satellite capabilities could contribute to aviation safety and efficiency, the National Aeronautics and Space Administration (NASA) developed an Advanced Satellite Aviation-weather Products (ASAP) initiative in 2002 to help transfer some of the new satellite observing systems and products into operational use through a collaborative effort with the FAA's existing Aviation Weather Research Program (AWRP).

The AWRP focuses on developing and enhancing aviation weather products that respond to the needs of users and FAA priorities. All new weather products developed by the AWRP's Product Development Teams (PDTs) go through extensive testing and evaluation, culminating in

a formal review by a joint FAA and NWS Aviation Weather Technology Transfer Board (AWTT) before they are declared operational and made available to the public. The AWTT review process puts an equal emphasis on high accuracy and low false alarm rates.

The NASA-funded ASAP initiative is structured to work with the AWRP's existing Product Development Teams to help fill critical gaps or to extend current products while making sure that the FAA is aware of the new capabilities that are becoming available and which may be ready for operational use (see Mecikalski et al. 2002). In general, the ASAP contributions to the PDTs will not result in stand-alone "satellite" products, but rather contributions towards integrated products that also incorporate multiple observing systems and numerical weather prediction model results.

Our paper highlights this highly complementary collaboration, beginning with an overview of the initiative in Section 2 and continuing with descriptions of the individual products in later sections.

## 2.0 ASAP Overview

ASAP is administered by the NASA Langley Research Center (LaRC) in close collaboration with the FAA's management of its AWRP efforts. The ASAP program is sponsored by the NASA Aviation Safety and Security Program (AvSSP) and the NASA Applied Sciences Program's Aviation Applications Program, whose goals to achieve broader societal impacts are also closely coordinated with the FAA (Murray 2002). Like the AWRP team members, the ASAP team represents a collaboration between university and government researchers with a specific goal of bringing together groups that are experienced in satellite

remote sensing, but who have not had a history of working on aviation-related problems, with researchers having long histories of studying aviation weather.

Current participants in the ASAP program include scientists and engineers at NASA's Langley Research Center (LaRC), the University of Alabama in Huntsville (UAH), the NOAA Cooperative Institute for Meteorological Satellite Studies at the University of Wisconsin (UW-CIMSS), the Massachusetts Institute of Technology Lincoln Laboratory (MIT-LL), and the National Center for Atmospheric Research (NCAR)<sup>2</sup>.

The ASAP effort is envisioned as two complementary phases. The first phase emphasizes enhancing the FAA's AWRP use of *current* satellite data and processing techniques, while the second phase will seek to identify aviation applications for the *next generation* of high spectral and spatial resolution satellite instruments and give aviation requirements a higher priority in future satellite planning. Appendix A outlines several of the anticipated advanced satellite instruments that will have capability for improving aviation weather diagnosis and forecasting, especially as aviation requirements gain a higher priority in future satellite planning. New satellite names and satellite-borne sensing systems that are not included in the AMS's Glossary of Meteorology, Second Edition, as provided in the Appendix.

In conjunction with the FAA's Product Development Teams, ASAP is working to identify areas where satellite data can fill gaps in weather products already under development and to propose new satellite-based "interest fields" that can be incorporated into integrated FAA weather products. ASAP includes efforts to improve cloud identification and properties, monitor the initial stages of developing convection, improve assessments of in-flight icing potential,

---

<sup>2</sup> See ASAP web sites at [cimss.ssec.wisc.edu/asap](http://cimss.ssec.wisc.edu/asap) (UW-CIMSS) and [nsstc.uah.edu/johnm/ci\\_studies.html](http://nsstc.uah.edu/johnm/ci_studies.html) (UAH). The NASA ASAP page is [asd-www.larc.nasa.gov/new\\_AtSC/asap.html](http://asd-www.larc.nasa.gov/new_AtSC/asap.html).

identify flight areas that are likely to be turbulent, and develop automatic algorithms to detect volcanic eruptions and identify hazardous areas of volcanic ash.

### 3.0 Basic Cloud Properties

Satellite products have become widely available and are an essential component of most modern meteorological analyses. For the most part, however, satellite data sets are only used in the form of simple cloud masks (cloud or no-cloud), cloud top heights, or other basic properties. Clouds can also be tracked for making wind estimates (Velden et al. 1997; 1998). While these seemingly simple parameters are widely used, improved satellite observing systems and new analysis techniques (e.g. Velden et al. 2005) can be combined to produce improved basic products (cloud masks, cloud classification analyses, and cloud top heights) that can be transferred directly, and quickly, to existing operational analysis systems.

While accurate observations of cloud top height are critical for many aviation applications, the specific products that are needed can vary from a simple statute height above ground level (or sea level), to a separate cloud top pressure product which is appropriate for *en route* aircraft flying above 18,000 ft (5625 m). These aircraft, which set their altimeters to a standard reference, display their flight levels in thousands of feet while they are actually flying along constant pressure surfaces.

For some time, satellite-based infrared sounders have been able to generate operational cloud top pressure fields through a multi-spectral CO<sub>2</sub> slicing technique (Wylie and Mendel 1989). These fields, however, have not been used to any great extent for aviation applications because of the relatively large sounder footprint along with the product's limited area coverage and slow update rates. With the launch of the GOES-12 Geostationary Operational

Environmental Satellite with a new 13.3  $\mu\text{m}$   $\text{CO}_2$  imaging channel, it has become possible to generate cloud top pressure fields using the higher resolution, rapidly updating GOES imager. In this case, the  $\text{CO}_2$  slicing technique has been adapted for use with the imager in a new,  $\text{CO}_2$  ratio technique (Schreiner and Schmit 2001; Bedka et al. 2005).

One of the advantages of the new  $\text{CO}_2$  ratio technique is to produce a better estimate of the height of thin, semi-transparent cirrus and other high clouds that are difficult to assign to a specific height because of contamination of the cloud information by the underlying surface temperature field. Unfortunately, the  $\text{CO}_2$  channel is limited to mid and upper level clouds. A full cloud top pressure product is therefore developed through the combination of height estimates from the  $\text{CO}_2$  ratio technique for the upper clouds and from the older “infrared (IR) window” technique for lower clouds (Schreiner et al.1993). The IR window technique is based on using the 11  $\mu\text{m}$  thermal IR temperature to estimate the temperature at cloud top, combined with an atmospheric sounding to convert the temperature value to a corresponding pressure and height. Figure 1 shows an example of this GOES imager-based cloud top pressure product.

Figures 2 and 3 show a detailed comparison between the GOES-12 Imager and Sounder cloud top heights (converted to statute height in this example), coupled with simultaneous observations by the NASA Cloud Physics Lidar (CPL), flying on the NASA ER-2 aircraft. These measurements were conducted in the winter of 2003 as part of the Atlantic THORPEX Regional Campaign (ATReC). Figure 2 shows the GOES-12 Imager (top-red) and GOES-12 Sounder (bottom-blue), as well as CPL (black) cloud-top heights from 5 December 2003. The Imager heights show better agreement with the CPL than the Sounder heights due to the increased spatial resolution of the Imager. The best agreement for both satellite instruments is for mid-level

clouds, while both the Sounder and Imager underestimate the CPL cloud-top height both for semi-transparent high clouds, and warm low-level clouds.

Figure 3 shows a histogram of the absolute differences between the CPL cloud top height and the GOES Imager (red) and Sounder (blue) cloud top height for 5 December 2003. This histogram indicates that the distribution of differences between both GOES products and the CPL is bell shaped with the peak in the 0.5 to 1 km bin. The distribution of differences for both satellite instruments shows a longer tail to the right, indicating that the satellites underestimate the CPL cloud top height more often than they overestimate it. For both instruments, a similar percentage (about 5.5% for the Sounder and 4.9% for the Imager) of the data points had absolute errors greater than 5 km (outside the histogram range). This result suggests that the cloud types for which height assignments are most difficult (for instance, optically thin, broken, or multi-layered clouds) are consistent for both broadband instruments. The root mean square and bias statistics for each satellite (summarized on the figure) confirm the better performance of the Imager derived product than the corresponding Sounder derived product.

#### 4.0 Convective Initiation

Thunderstorms account for most of the air traffic delays in the U.S. and cost the aviation industry many millions of dollars annually in lost time, fuel and efficiency through delayed, cancelled and rerouted flights (Kaplan et al. 1999; Murray 2002). In response to this need, the FAA's Convective Weather Product Development Team is working to develop reliable 0-8 hour probability forecasts of convective weather and automated 0-2 hour high-resolution deterministic forecasts over the continental United States.

Historically, much of the Convective Weather PDT's work has centered on the use of weather radars to monitor convective storm development. Radars, however, do not see the early stages of convective cloud formation and growth. The ASAP team is currently working with the FAA Convective Weather PDT to develop and transfer satellite-based techniques for detecting, tracking, and monitoring the early development of small cumulus in order to improve thunderstorm initiation forecasts.

The first step in the ASAP satellite-based convective initiation (CI) product is a new convective cloud identification system, the "convective cloud mask" or CCM. The CCM relies on an unsupervised statistical clustering algorithm (Berendes et al. 2005) to classify the cloud features in satellite imagery based on the methodology of Nair et al. (1998). The iterative clustering algorithm groups pixels into clusters based upon a statistical similarity measure (Levine and Shaheen 1981). The clustering algorithm was trained using GOES data over the continental United States. All of the GOES channels were used as features. In addition, the contrast texture measure of channel 1 (visible) was used as a training feature for the clustering algorithm.

While the CCM can be used with both geostationary and polar-orbiting satellite systems, its application to convective initiation requires monitoring the cloud imagery over time and is best suited for use with GOES imagery updated every 15 or 30 minutes. The CCM is optimized for identifying small convective clouds through the use of both 1-km resolution visible imagery and 4-km resolution infrared imagery, with the cloud mask being produced at 1-km resolution. This means that the CCM is only available during daylight hours. In spite of its high resolution, the CCM's emphasis on non-precipitating convective clouds simplifies the processing and allows it to be applied over large geographical areas.

Figure 4 shows the clustering results for a GOES image over the central U.S. Large-scale convective complexes are visible along with smaller cumulus and stratiform clouds. The classifier is able to detect the smaller convective clouds. Additionally, the isolated overshooting cumulus tops can be seen in red.

Convective clouds identified by the CCM are then tracked using a modified version of the Velden et al. (1997; 1998, and 2005) atmospheric motion vector (AMV) algorithm. The modified version is optimized for mesoscale studies by reducing its dependence on first-guess motion estimates from numerical weather prediction models. This approach results in a higher density of cloud motion vectors that includes *both* synoptic and mesoscale forcing, as discussed in Bedka and Mecikalski (2005).

Motion vectors are computed by identifying cloud “targets” across an image sequence through the use of advanced pattern-matching techniques and cross-correlation statistics (Merrill et al. 1991). With the relaxed constraints to synoptic-scale forcing, the number of AMVs calculated can increase significantly (as much as a 20-fold increase in motion vectors that pass quality control filtering), giving a better depiction of the mesoscale flow patterns that can influence convective initiation. Figure 5 shows the increased coverage of the height-stratified satellite-derived motion vectors using this analysis technique.

By combining the convective cloud mask and the corresponding atmospheric motion vectors, it is possible to monitor the changing cloud properties for individual small cumulus. These tendencies can then be monitored for signals of cloud growth. Cloud-top cooling rates, for example, are a good general indication of cloud development. Roberts and Rutledge (2003) showed that the occurrence of sub-freezing  $10.7 \mu\text{m}$  brightness temperatures coupled with cooling rates of  $8^\circ\text{C}$  in 15 minutes provided up to 30 minutes of advance notice of the

development of cumulonimbus with radar reflectivities of 35 dBZ or greater. Figure 6 illustrates the calculated cooling rates for areas of developing convection in the Midwest.

Mecikalski and Bedka (2005) have extended these tendency techniques to a variety of multispectral band differences from GOES imager data to produce eight predictor fields that can be used to characterize cloud conditions consistent with convective initiation. The fields are (1) 10.7  $\mu\text{m}$  cloud top brightness temperature, or  $T_B$ , (2 and 3) cloud top  $T_B$  cooling rates at 15 and 30 minutes, (4) cloud top  $T_B$  temperatures dropping below  $0^\circ\text{C}$ , (5 and 6) the 6.5 minus 10.7  $\mu\text{m}$  channel difference as discussed by Ackerman (1996) and its time rate of change, and (7 and 8) the 13.3 minus 10.7  $\mu\text{m}$  channel difference and its time rate of change. After selecting suitable thresholds for these growth trend indicators, Mecikalski and Bedka generate a satellite-based, summary convective initiation product defined by small clouds that meet at least 7 of the 8 growth criteria. The results of this type of analysis are shown in Figure 7, where the red pixels represent small convective clouds that have been identified as being likely to develop  $\geq 35$  dBZ radar echoes within the next hour. The FAA's Convective Weather PDT is evaluating this satellite-based convective initiation product, along with its individual trending components, for inclusion in their short-term (0-6 hour) forecast systems. Figure 8 shows an example of the ASAP cloud-top cooling field as used within this forecast system.

## 5.0 In-flight Icing

Aircraft penetrations of supercooled clouds can result in a rapid build up of ice on the aircraft wings and control surfaces. In extreme conditions this ice build up has been directly responsible for airplane crashes. On 31 October 1994, for example, an ATR-72 commuter airline crashed in Roselawn, Indiana, killing all 68 persons on board following a build up of ice on the

wings and airframe. While the microphysical conditions that result in in-flight icing hazards are generally well understood, it has proved challenging to develop reliable techniques for operationally diagnosing icing conditions or forecasting their occurrence. For many years the FAA has sponsored the development of advanced techniques to identify icing hazards and alert pilots to the danger. These techniques rely on a variety of data sources including radar, satellite, surface observations, and pilot reports as well as predictions from high-resolution, rapidly updated numerical weather prediction models. At present, the most sophisticated operational icing product is the Current Icing Potential (CIP; Bernstein et al. 2005), developed by the FAA's In-flight Icing Product Development Team and run operationally by the National Weather Service. The current operational version of CIP makes relatively limited use of satellite data, using multiple channels to develop a 3-D cloud mask. The ASAP program intends to enhance CIP through the use of advanced satellite products.

Satellite-based methods using combinations of visible reflectance and infrared emittance can be used to estimate cloud properties such as hydrometeor size and liquid water path (LWP). Ellrod and Nelson (1996), Vivekanandan et al. (1996), and Minnis et al. (2001) have suggested that in addition to characterizing the location, size and depth of cloud systems, satellite observations can be used to monitor the cloud-top phase (i.e. ice or liquid), water content, and droplet diameter—all properties that are of interest in diagnosing possible icing conditions. Although satellite-based cloud retrievals using the visible and infrared spectral bands can only monitor conditions over a limited depth at the top of the cloud, these techniques have shown skill in monitoring hydrometeor size and phase information in that region. In some cases the cloud top regions may even be of special interest since the largest amounts of supercooled liquid water are often found within several hundred meters of the top of layered stratiform and convective

clouds (Hobbs and Rangno 1986; Rauber and Tokay 1991). While cloud top information from satellite retrievals can be valuable, stand-alone satellite products must be used with caution since the hydrometeors at cloud top are not always typical of those below. For general use, satellite techniques need to be integrated with other observational systems and model output, such as those employed by CIP.

The ASAP icing team is currently evaluating GOES-derived cloud products developed at NASA Langley Research Center (LaRC; Minnis et al. 2001) for integration into the FAA's operational CIP system. These products are generated with the Visible Infrared Solar-infrared Split-window Technique (VISST) during the daytime and with the Solar-infrared Split-window Technique (SIST) at night (Minnis et al. 1995; 1998). Each 4-km GOES pixel is first classified as clear or cloudy using a sophisticated cloud identification scheme (Trepte et al. 1999). Multi-spectral VISST/SIST algorithms are then applied to each cloud pixel to determine cloud phase, optical depth, effective particle size, effective temperature, effective height, and ice or liquid water path.

In collaboration with the FAA's In-flight Icing PDT, the ASAP icing team has been testing NASA LaRC cloud products as a nowcasting tool for guiding research aircraft into areas with the greatest potential for icing. The satellite-derived cloud products, in conjunction with other standard meteorological information, have already been used in support of the NASA Glenn Research Center icing research flight program (Wolff et al. 2005) and the 2005 Alliance Icing Research Study (Isaac et al. 2005). In these experiments, satellite-derived phase, liquid water path (LWP), and effective radius ( $R_e$ ) were used to identify areas with possible icing conditions to guide research aircraft to collect *in situ* observations. The aircraft observations, in turn, can be used to evaluate the NASA LaRC products.

For example, on 19 January 2005 forecasters targeted clouds over central and western Ohio because of a combination of supercooled liquid phase cloud tops, relatively high LWP values of 800-1000  $\text{gm}^{-2}$ , and  $R_e$  values on the order of 10  $\mu\text{m}$  (see Figure 9). Widespread cloudiness covered the region on this day. The limited cloud-free areas in the figure are colored black. Clouds with glaciated tops are colored gray. Upon reaching the area, the aircraft encountered liquid water contents measuring 0.4-0.6  $\text{gm}^{-3}$ . These values were very close to those anticipated from the satellite-derived liquid water path estimates, and in situ observations of mean volume drop-size diameters ( $\sim 15 \mu\text{m}$ ) were in good agreement with  $R_e$  estimates ( $\sim 10 \mu\text{m}$ ). During earlier portions of this flight made along the Ohio-West Virginia border, liquid water contents observations did not match the values expected from the LWP estimates nearly as well (0.2-0.3  $\text{gm}^{-3}$  with LWP of 700-1000  $\text{gm}^{-2}$ ). This discrepancy may be explained by the presence of large  $R_e$  values ( $>20 \mu\text{m}$ ) at cloud top. Since the VISST algorithm calculates LWP using the cloud-top  $R_e$  value, it may overestimate LWP if the cloud-top  $R_e$  value is larger than particle sizes in lower parts of the cloud (Khayer et al. 2003). Note that the aircraft did encounter larger drop sizes during this portion of the flight.

After three seasons of using the NASA LaRC products, field program forecasters have found them to be quite useful and have developed their own “rules of thumb” for when specific products are of value. For example, large areas with uniform values of phase, LWP, or  $R_e$  are usually more reliable indicators of icing conditions than areas with high spatial variability. Gradients in LWP that are embedded within widespread stratiform clouds are usually found to be accurate at least in a qualitative sense, while sharp transitions are sometimes problematic. Cloud-top phase estimates are typically quite good, and higher  $R_e$  estimates correlate well with in situ observations of larger drops (Haggerty et al. 2005).

The ASAP icing group is currently conducting more comprehensive validation studies using research aircraft data and pilot reports, as well as comparisons with the current generation of CIP output. The forecasters' observations and insights, in combination with these more comprehensive validation studies, are providing direction to the creation of specific rules and procedures for integrating the advanced satellite-derived measurement fields into a new, high-resolution CIP product that will focus on expected icing severity.

## 6.0 Turbulence

Turbulence has long been considered a priority problem for commercial aircraft, and is the single greatest cause of injuries to flight crew and passengers as well as having the potential to cause structural damage to aircraft. Turbulence affecting aircraft is a small-scale phenomenon with length scales of tens to hundreds of meters. This makes it particularly difficult to observe with conventional observing systems, models, or satellites. It may be possible, however, to use satellite observations to identify larger scale features or conditions that can lead to clear air or convectively induced turbulence. In this case, the satellite "products" or "interest fields" would need to be integrated with other observational systems and model output to produce an operationally useful warning product.

One common source of turbulence is from breaking waves associated with flow over mountains or other terrain features. Wave clouds can often be observed in high-resolution satellite imagery, but the mere presence of wave structures is by itself not necessarily an indication of a turbulence hazard. In addition, mountain waves do not always generate clouds. Wave structures in clear air can sometimes be observed in high-resolution water vapor imagery, where the wave motions result in humidity patterns that mimic the appearance of wave clouds

(see Fig. 10). As part of ASAP, we are working on the development of an automated mountain wave identification algorithm for clouds and water vapor features that can be used with either GOES or MODIS imagery. Our current approach examines the water vapor channel for sudden changes in the magnitude and direction of the gradient by applying Laplacian of Gaussian (LoG) filtering. In our wave detection application of the LoG filter, the “edges” correspond to sudden changes in water vapor content. The sigma value used in the LoG filter affects the wavelength of the wave patterns enhanced by the LoG filter. Larger sigma values enhance larger wavelengths while smaller  $\sigma$  values enhance shorter wavelengths.

Changes in water vapor gradient direction are determined by finding the points in the LoG image where the sign changes between neighboring pixels. This “zero crossing” point represents a change in water vapor gradient direction that could be an indicator of turbulence.

Figure 10 shows an example using a MODIS image over an area in Colorado where a pilot reported turbulence within 30 minutes of the MODIS overpass. Wave patterns are clearly visible in the contrast-enhanced 6.7  $\mu\text{m}$  channel shown in Figure 10a. The zero crossing of the LoG image can be seen in Figure 10b. The wave patterns are clearly detected. Brighter pixels represent a higher magnitude gradient difference across the zero crossing point, and therefore more likely regions of turbulence.

The LoG method should be able to be used to quantify the strength and direction of mountain waves at different wavelength scales. By combining the LoG method with other image processing and pattern recognition techniques, we hope to quantify the overall wave structure and find the relationship between the water vapor wave patterns and turbulence. This same technique may also be suitable for identifying gravity waves produced by convective clouds or systems, as modeled by Lane et al. (2003). In this case the wave detection capabilities would be

used in conjunction with a generalized convective cloud mask (CCM) to identify strong updrafts based on the cloud-top cooling rates. In combination with other observational systems and model output fields, this information may be able to help identify areas of convectively induced turbulence (CIT).

Another example of a satellite-derived turbulence interest field is a product that identifies areas of tropopause folding, where the lower boundary of the stratosphere folds down into the troposphere. These folds frequently lead to dynamical instability that can result in areas of enhanced turbulence (Gidel and Shapiro 1979; Shapiro 1980). To this end, a turbulence prediction tool has been developed based on an upper-tropospheric specific humidity product that is derived from the GOES water vapor channel and corrected for satellite viewing angle and temperature (Moody et al. 1999; Wimmers and Moody 2001). The specific humidity product, termed GOES Layer Average Specific Humidity or GLASH, varies closely with tropopause height. Strong gradients in the GLASH field have been found to be associated with tropopause folding (Wimmers et al 2004a; 2004b). Figure 11 illustrates a GLASH field over the United States. Areas of yellow and red indicate subtropical air, while areas of blue and purple identify areas of dry polar air. Estimated areas of tropopause folding are represented as gray ribbons of uniform width, based on an assumed average size of tropopause folds. As a turbulence “interest field” this sort of product is integrated with model-generated fields to assign height limits for the folding, and to put this possible source of turbulence into a broader context.

In a longer-term effort, the ASAP science team is conducting an observing system simulation experiment (OSSE) to evaluate the potential for future hyperspectral sounding systems—such as currently planned for the National Polar-Orbiting Operational Environmental Satellite System (NPOESS) Preparatory Project (NPP), and GOES-R (Schmit et al. 2005)

satellites—to infer the presence of turbulence. In this experiment, NCAR scientists are generating three-dimensional output fields from very high-resolution numerical models that are capable of resolving the onset and development of turbulence on scales of importance to aircraft. These three-dimensional data fields will then be used by researchers at UW-CIMSS as “ground truth” for a simulation of the expected hyperspectral signals that will be observed by advanced high spectral resolution infrared sounders, such as CrIS, IASI, and HES (see Appendix A). All hyperspectral instruments will be capable of observing/measuring atmospheric features at unprecedented vertical resolution, with an ability to resolve small or moderate scale temperature or water vapor perturbations through evaluation of many channels. While the current GOES Sounder footprint may be too large to detect turbulent structures directly (~8-10 km), these new hyperspectral instruments will have the capability to identify areas of high wind-shear or high spatial variability in temperature and humidity and through the monitoring of the returned signals with time or by tracking the motion of larger-scale features that may be associated with turbulence. This information, when used in conjunction with other turbulence observations and diagnostics from numerical weather prediction models, may become an important contribution to an integrated turbulence forecasting system.

## 7.0 Volcanic Ash

Inadvertent penetrations of volcanic ash clouds have caused several nearly catastrophic commercial airline incidents, including engine failures from particulate ingestion and the total obscuration of cockpit windscreen from etching by the acidic aerosols (Miller and Casadewall 2000). The international community has established a network of Volcanic Ash Advisory Centers (VAAC) that are responsible for monitoring the air space in their assigned geographical

regions for hazardous eruptions and to issue warnings as needed to all aircraft in their respective areas (Romero 2004). At present, the VAACs make use of satellite observations, pilot reports, and alerts received from volcano observatories and ground-based monitoring systems. The FAA's Oceanic Weather PDT is working to assist the VAACs through improved detection and processing systems. In support of the FAA's contributions, the ASAP team is working with the PDT to develop and test advanced, satellite-based volcanic ash detection techniques for higher reliability, earlier detection, fewer false alarms, and better identification of the plume height.

While ash clouds are sometimes quite impressive in visible satellite imagery, it is frequently difficult to distinguish ash clouds from natural, non-volcanic water and ice clouds. Fortunately, suspended ash particles have some distinct spectral signatures that can be used to enhance their detection through multi-spectral image processing. The most commonly used multi-spectral technique is based on a strong 12- $\mu\text{m}$  absorption signature (e.g. Prata 1989), which causes a negative 11- $\mu\text{m}$ —12- $\mu\text{m}$  brightness temperature difference. This technique is often termed the reverse absorption method, and has been the basis for a number of different detection techniques, as discussed by Ellrod *et al.* (2003).

In addition to ash, volcanic eruptions usually release high concentrations of  $\text{SO}_2$ , which has strong absorption bands at 7.3 and 8.6  $\mu\text{m}$ . While the ash cloud and the  $\text{SO}_2$  plume do not always follow the same down-wind trajectories (e.g. Seftor et al. 1997), the presence of an  $\text{SO}_2$  plume can help confirm a volcanic eruption and improve the reliability of complementary algorithms, such as those based on reverse absorption methods. At present,  $\text{SO}_2$  absorption channels are available on the high-resolution MODIS imager and the AIRS sounding instrument in polar orbit on NASA's EOS satellites, with the next generation operational geostationary satellite (e.g., GOES-R) having similar capabilities.

ASAP efforts to enhance volcanic ash detection are concentrated on improving satellite-based multi-spectral techniques for identifying and tracking ash clouds and for estimating their height. Once demonstrated and evaluated, these techniques will be transferred to the VAACs.

Volcanic eruptions and the resultant ash plumes can exhibit considerable variability in their structure and composition — with potentially variable responses to different detection algorithms. While individual detection techniques can often enhance the visibility of the ash plume, the resultant images are themselves somewhat noisy and prone to false detections. To minimize these problems we have concentrated on techniques that may be able to reduce the number of false alarms, either by the integration of results from multiple detection algorithms or through the inclusion of additional satellite channels that might provide a more robust detection capability. In much of our volcanic ash work we have emphasized the use of MODIS imagery as our primary test bed since MODIS provides observations at most wavelengths of potential interest and very high spatial resolution.

ASAP ash detection studies are currently underway at UW-CIMSS and UAH. One approach being investigated is based on the standard reverse absorption technique supplemented with visible (0.65  $\mu\text{m}$ ) and near-infrared (3.75  $\mu\text{m}$ ) channel data (Pavolonis et al. 2005). This new technique is physically-based and globally applicable. Unlike the reverse absorption technique, the new algorithm does not require the presence of a negative 11- $\mu\text{m}$  minus 12- $\mu\text{m}$  brightness temperature difference that is often absent, especially in tropical eruptions. Figure 12 shows the results of applying both the Pavolonis et al. algorithm and the standard reverse absorption technique to a 2004 eruption of Manam in Papua New Guinea. The new approach is able to identify ice clouds that are heavily contaminated with volcanic aerosols even though these clouds generally lack a reverse absorption signature. The reverse absorption results only

detect the portions of the low level ash plume that are quite near the volcano, while having many small areas of negative brightness temperature difference showing up in the nearby convective clouds. In contrast, the new algorithm produces a clean, false alarm-free integrated product.

In a separate effort, the same statistical clustering approach used in the convective cloud mask, discussed in Section 4 (Berendes et al. 2005), is applied to ash detection. The clustering algorithm makes use of MODIS channels that are known to be useful for detecting volcanic ash (0.65  $\mu\text{m}$ , 0.55  $\mu\text{m}$ , 3.75  $\mu\text{m}$  reflectance and brightness temperature, 11.0  $\mu\text{m}$ ). In addition, several difference channels (11–12  $\mu\text{m}$ , 3.75–11  $\mu\text{m}$ ) were selected for inclusion based upon a principal component analysis (Hilger and Clark 2002). Finally, a ratio channel (3.7  $\mu\text{m}$  reflectance / 0.65  $\mu\text{m}$ ) was added to the cluster (Pavolonis et al. 2005).

The Berendes et al. (2005) clustering algorithm was trained using several days of data over the Manam volcano and five clusters out of approximately 160 were identified as containing volcanic ash. Figure 13 shows a true color MODIS image of the Manam volcano in the upper left. The clusters are shown upper right using a randomized color scheme. The lower left-image in Fig. 13 shows the thresholded 3.7/0.65  $\mu\text{m}$  and the lower right image shows the volcanic ash clusters in red. The volcanic ash clusters correspond well with the ash areas indicated by the 3.7/0.65  $\mu\text{m}$  image; one drawback is that ice-clouds contaminated with ash are not well identified by this method.

This clustering technique has shown considerable potential for producing clean identification of prominent ash plumes over both land and water, but requires regional training and, like many techniques, has difficulty with optically thin ash plumes. Recent developments in the clustering algorithm have allowed for the creation of texture channels that can be used as

features for training the clustering. Textural clustering may yield significant improvements in the detection of thin, dry ash, especially over land.

Identifying the height of an ash cloud can be very difficult, particularly when the ash is semi-transparent. At operational VAAC centers, plume height identification is performed by observing plume drift and correlating with global model wind fields at various altitudes. When the atmosphere exhibits directional shear, this can be a very accurate approach, but it cannot be relied upon for all situations.

ASAP height identification efforts are based on two potential retrieval algorithms: 1) the CO<sub>2</sub> ratio technique applied to MODIS data (Platnick et al. 2003) and, 2) a “split-window” (e.g. 11 μm and 12 μm regions) 1D-VAR retrieval (e.g. Marks and Rodgers 1993; Heidinger et al. 2005). The MODIS CO<sub>2</sub> ratio technique utilizes the four CO<sub>2</sub> absorption channels on the MODIS (channels 33 – 36) in a conceptually consistent manner as described in Section 3. The split-window technique operates under the premise that for a known atmospheric state, the split-window measurements for a single layer cloud are primarily determined by three factors: (1) cloud temperature, (2) cloud emissivity, and (3) cloud particle size and shape distribution. If an ash cloud is identified by the four-channel technique or some other method, a reasonable assumption about the particle size and shape characteristics can be made, leaving only the cloud temperature and emissivity to be retrieved within the 1D-VAR system from the measured 11-μm and 12-μm radiances. The resultant cloud temperature can then be matched to a pressure or height within an atmospheric sounding as is performed in the CO<sub>2</sub> ratio technique.

Although the CO<sub>2</sub> slicing method should be more accurate than the split-window method for mid and upper tropospheric plumes, many imagers do not (and will not) have CO<sub>2</sub> absorption

channels, so the split window algorithm may be a useful substitute when CO<sub>2</sub> slicing is not possible. For lower tropospheric ash plumes the split window method should be superior.

The use of MODIS imagery limits the likely operational use of many of these techniques to real-time demonstrations, based on the need for prompt availability of the data at the VAAC. With the launching of the GOES-R series of operational geostationary satellites, however, these same techniques should be readily transferred to full operational use.

No matter how reliable our ash identification techniques become, or how well we can track and predict the spread of the ash cloud, it is critical that the initial alerts and warnings be issued rapidly. At the 2004 Conference on Volcanic Ash and Aviation Safety in Alexandria, Virginia, for example, it was noted that volcanic ash can reach commercial flight levels in as little as five minutes. Even with extensive monitoring systems currently in place at key volcanoes and an international network of VAACs, it can take hours for eruptions in remote areas to be identified, evaluated, and for formal alerts to be issued.

In order to speed the initial detection of explosive eruptions, ASAP investigators are also examining untraditional approaches, such as using Department of Defense's infrared surveillance satellites. These satellites are the backbone of the global missile early warning system and make observations of the Earth in the short wave infrared regions, with 10-second resolution. DoD scientists have documented the detection of volcanic eruptions in this imagery and have reported evidence of a good correlation between the strength and duration of the initial signal "spike" and the magnitude of the explosive eruption and the attendant plume height (Pack et al. 2000).

DSP imagery, if processed routinely for volcanic eruptions and made available to the VAACs, may be a uniquely valuable enhancement to existing volcano monitoring systems and would permit rapid analysis of eruptions that could prove to be a threat to aviation.

## 8.0 Summary

The fundamental objective of the ASAP program is to support the existing FAA weather Product Development Teams, to encourage full use of existing and future satellite-based observing systems for aviation applications, and to accelerate the transition of research products to operational use.

Observations and products from research satellites, however, are not always appropriate for routine operational use. Data access can be slow and one-of-a-kind satellites like Aqua and Terra are only overhead at certain times of the day. These satellites, however, can play an important role in validating current weather products with researchers gaining experience in the use of their advanced sensors in the process.

In many cases research sensors also serve as prototypes for future operational sensing systems. NASA's MODIS imager, for example, can be considered the prototype for both upcoming NPP and NPOESS Visible Infrared Imagery/Radiometer Suite (VIIRS) satellites, as well as the GOES-R Advanced Baseline Imager (ABI). Experience with the research instruments will translate directly to accelerated use of the upcoming operational instruments with already tested products.

### Acknowledgments

Research support for the Advanced Satellite Aviation-weather Products (ASAP) initiative was provided by the NASA Applied Sciences Program under the direction of Ronald Birk and by the NASA Aviation Safety and Security Program's (AvSSP) Aviation Weather Information element directed by Paul Stough.

ASAP efforts are dependent on the coordination and cooperation of the Federal Aviation Administration's Aviation Weather Research Program (FAA-AWRP), under the direction of Ms. Gloria Kulesa. We also gratefully acknowledge the input and guidance we have received from the FAA's Product Development Teams, including the teams for In-flight Icing (Marcia Politovich, NCAR), Turbulence (Bob Sharman, NCAR), Convective Weather (Marilyn Wolfson, MIT-LL, and Cindy Mueller, NCAR), Oceanic Weather (Cathy Kessinger, NCAR), and National Ceiling and Visibility (Paul Herzegh, NCAR). We also gratefully appreciate the assistance of John Haynes (NASA) on the ASAP initiative.

## APPENDIX A:

### Appendix: Glossary of new satellite and satellite-borne observing systems.

This appendix is intended to update the AMS's Glossary of Meteorology, Second Edition to reflect new satellites and instruments that are not included in the current version of the glossary. References to terms already defined in the *Glossary of Meteorology, Second Edition* are printed in blue, bold-face type and underlined.

**ABI**—Abbreviation for **Advanced Baseline Imager**. ABI is a 16 channel high-resolution imager covering visible, short, mid- and long-wavelength **infrared** spectral regions. The visible and **near-infrared** channels will provide 500 m (one channel only) or 1 km resolution imagery at **nadir**, while the remaining mid infrared channels will have a nadir resolution of 2 km.

**AIRS**—Abbreviation for **Atmospheric Infrared Sounder**. AIRS is a hyperspectral sounder flying on the **Earth Observing System** satellite **Aqua**. AIRS is based on a grating spectrometer that produces over 2,000 bands of data to provide accurate temperature and humidity profiles throughout the atmosphere. AIRS also provides measurements of cloud optical thickness and total column ozone.

**CrIS**—Abbreviation for **Cross-track Infrared Sounder**. A **Michelson Interferometer**-based **hyperspectral sounder** that is similar to the **AIRS** sounding instrument on **EOS Aqua**. CrIS will be flown on the upcoming **NPP** and **NPOESS** satellites, providing high-accuracy temperature and moisture profiles in cloud free areas using over one thousand spectral channels of information in the **infrared**.

**Earth Observing System**—(Abbreviated EOS.) A major NASA initiative to develop state-of-the-art **remote sensing** instruments for global studies of the land surface, **biosphere**, solid earth, **atmosphere**, and oceans. EOS is built around three major satellite platforms polar, **sun-synchronous** orbits. **Terra** has a mid-morning **descending node** crossing time, while the other two main EOS satellites (**Aqua** and **Aura**) share a common orbit with a series of complimentary earth observing satellites (termed the **A-Train**) with an early afternoon **equator** crossing time. Each EOS satellite is designed to make maximum use of simultaneous views of the earth from a wide variety of instruments.

**GOES-R**—Abbreviation for the “R” series of **Geostationary Operational Environmental Satellites**, tentatively scheduled for launch and deployment beginning in 2012. These new satellites will provide greatly enhanced observational capabilities through a series of new observing systems including an advanced geostationary imager (**ABI**) and a hyperspectral sounder (**HES**).

**HES**—Abbreviation for **Hyperspectral Environmental Suite**. HES is a new sounding instrument that will provide improved spatial coverage, faster scanning speeds, and a smaller sensing **footprint**. HES is a **hyperspectral sounder** that will be able to resolve over 3000 spectral channels of information in the **infrared**. This high spectral resolution will provide increased accuracy and higher vertical resolution soundings.

**IASI**—Abbreviation for **Infrared Atmospheric Sounding Interferometer**. IASI is a **hyperspectral sounding** system that will be flown on the METOP series of satellites. IASI uses an imaging Fourier Transform Spectrometer in conjunction with a Michelson Interferometer to measure the infrared spectrum emitted by the earth. IASI will provide improved infrared soundings of the temperature profiles in the **troposphere** and lower **stratosphere**, moisture profiles in the troposphere, and observations of total column content of ozone, CO, CH<sub>4</sub>, and N<sub>2</sub>O.

**METOP**—The name given to the satellites to be flown as part of the EUMETSAT Polar System (EPS). These satellites, to be launched beginning in 2006, will be the first European operational meteorological satellites in polar orbit. The satellites will be placed in a sun-synchronous orbit with a mid-morning equatorial crossing time intended to compliment and extend the coverage provided by the U.S. **POES** system of meteorological satellites. METOP instrumentation will include an **AVHRR** imager, an advanced **TOVS** vertical sounding suite, an Infrared Atmospheric Sounding Interferometer (**IASI**), and additional sensors for measuring atmospheric ozone and near-surface wind vectors over the ocean.

**MODIS**—Abbreviation for **Moderate Resolution Imaging Spectroradiometer**. MODIS is a ground braking, high-resolution visible and infrared imager installed on two **Earth Observing System** satellites (**Aqua** and **Terra**). MODIS produces simultaneous images in 36 spectral bands with the individual bands having spatial resolutions at **nadir** ranging from 250 m (bands 1-2) to 500 m (bands 3-7) and 1000 m (bands 8-36). MODIS has a cross track imaging swath of 2330 km.

**NPOESS**—Abbreviation for **National Polar-orbiting Operational Environmental Satellite System**. NPOESS is the next generation of operational polar-orbiting satellites to be operated by the United States. NPOESS will combine the capabilities of the existing civilian **POES** satellites and the **DMSP** military satellites. The eventual system will consist of three separate satellites in **sun-synchronous orbits** with equatorial crossing times of 0530, 0730, and 1330 local solar time. NPOESS instrumentation will include the four instruments, **VIIRS**, **CrIS**, **ATMS**, and **OMPS**, that will be tested on the upcoming **NPP** satellite as well as a variety of other instruments. The first NPOESS satellite is not expected to be launched until 2010-2012.

**NPP**—Abbreviation for **NPOESS Preparatory Project**. The NPP is a risk reduction program that will launch a polar-orbiting meteorological satellite in a **sun-synchronous orbit** as a **NPOESS** precursor that will test four critical sensors (**VIIRS**, **CrIS**, **ATMS**, and **OMPS**) and new ground control, command, and communication segments that will be used with the operational **NPOESS** satellites. The NPP satellite is currently expected to be launched in late 2007 or 2008.

**VIIRS**—Abbreviation for **Visible/Infrared Imager Radiometer Suite**. The VIIRS instrument is a 22 channel high-resolution imager covering visible, short, mid-, and long-wavelength infrared spectral regions. VIIRS, which will be flown on **NPP** and **NPOESS** satellites, is based on the **MODIS** spectroradiometer used on NASA's **Terra** and **Aqua** satellites. VIIRS will have a resolution of 370 m at [nadir](#) and maintain a near constant horizontal resolution across its ~3000 km imaging swath.

## References

- Ackerman, S. A., 1996: Global satellite observations of negative brightness temperature differences between 11 and 6.7  $\mu\text{m}$ . *J. Atmos. Sci.*, **53**, 2803-2812.
- Barnes, S. L., 1964: A technique for maximizing details in numerical weather map analysis. *J. Appl. Meteor.*, **3**, 396-409.
- Bedka, K. M., and J. R. Mecikalski, 2005: Application of satellite-derived atmospheric motion vectors for estimating mesoscale flows. *J. Appl. Meteorol.* **44**, 1761-1772.
- Bedka, S. T., W. F. Feltz, A. T. Schreiner, and R. E. Holz, 2005: Satellite derived cloud top pressure product validation: Using aircraft based cloud physics lidar data from the AtREC field campaign. *Intern. J. Rem. Sensing*, In press.
- Berendes, T. A., J. R. Mecikalski, and U. S. Nair, 2005: A cluster-based feature classification algorithm for satellite imagery: Convective cloud and volcanic ash cloud delineation. In preparation. *J. Geophys. Res.*
- Bernstein, B., F. McDonough, M. Politovich, B. Brown, T. Ratvasky, D. Miller, C. Wolff, and G. Cunning, 2005: Current Icing Potential (CIP): Algorithm description and comparison with aircraft observations. *J. Appl. Meteorol.*, In press.
- Ellrod, G. P., 1996: The use of GOES-8 multispectral imagery for the detection of aircraft icing regions. Preprint, *8th Conf. on Satellite Meteorology and Oceanography*, January 28-February 2, 1996, Atlanta, Georgia, Amer. Meteor. Soc., Boston, pp. 168-171.
- Ellrod, G. P., B. H. Connell, and Hillger, D. W., 2003: Improved detection of airborne volcanic ash using multi-spectral infrared satellite data. *J. Geophys. Res.*, **108** (D12), 4356-4368.

- Fujita, T.T., 1985: *The Downburst*. Satellite and Mesometeorology Research Project (SMRP), University of Chicago, 122 pp.
- Fujita, T.T., 1986: *DFW Microburst*. Satellite and Mesometeorology Research Project (SMRP), University of Chicago, 155 pp.
- Gidel, L. T. and M. A. Shapiro, 1979: The role of clear air turbulence in the production of potential vorticity in the vicinity of upper tropospheric jet stream-frontal systems. *J. Atmos. Sci.*, **36**, 2125-2138.
- Haggerty, J. A., G. Cunning, B. Bernstein, M. Chapman, D. Johnson, M. Politovich, C. Wolff, P. Minnis, and R. Palikonda, 2005: Integration of advanced satellite cloud products into an icing nowcasting system. *World Weather Research Programme Symposium on Nowcasting and Very Short Range Forecasting*, Toulouse, France, 5 – 9 September.
- Heidinger, A. K., M. D. Goldberg, D. Tarpley, A. J. Jelenak, and M. J. Pavolonis, 2005: A new AVHRR cloud climatology. International Asia-Pacific Environmental Remote Sensing Symposium, *4th Remote Sensing of the Atmosphere, Ocean, Environment, and Space*, Honolulu, Hawaii, 8-11 November 2004. *Applications with Weather Satellites II* (proceedings). Bellingham, WA, International Society for Optical Engineering, (SPIE), 197-205.
- Hobbs, P.V., and A. Rangno, 1985: Ice particle concentrations in clouds. *J. Atmos. Sci.*, **23**, 2523-2549.
- Isaac, G. et al., 2005: First results from the Alliance Icing Research Study II. Proc. *43<sup>rd</sup> AIAA Aerospace Sciences Meeting*, Reno, Nevada, USA, 11-13 January.
- Kaplan, M.L., Y-L. Lin, A.J. Riordan, K.T. Waight, K.M. Lux, and A.W. Huffman, 1999: Flight safety characterization studies, part I: turbulence categorization analyses. Interim

Subcontractor Report to Research Triangle Institute, NASA contract NAS1-99074.

Khaiyer, M., P. Minnis, B. Lin, W.L. Smith, Jr., and A.D. Rapp, 2003: Validation of satellite-derived liquid water paths using ARM SGP microwave radiometers. Proc. 13<sup>th</sup> ARM Science Team Meeting, Broomfield, CO, Mar 31-Apr4.

Lane, T. P., R. D. Sharman, T. L. Clark and H. M. Hsu, 2003: An investigation of turbulence generation mechanisms above deep convection. *J. Atmos. Sci.*, **60**, 1297-1321.

Levine, M. D., and Shaheen, S. I., 1981: A Modular Computer Vision System for Picture Segmentation and Interpretation, *IEEE Trans. on Pattern Analysis and Machine Intelligence*, Vol. PAMI-3 (5), 540-556.

Marks, C. J. and C. D. Rodgers, 1993: A retrieval method for atmospheric composition from limb emission measurements. *J. Geophys. Res.*, **98**, 14939–14952.

Mecikalski, J. R., D. B. Johnson, J. J. Murray, et al., 2002: NASA Advanced Satellite Aviation-weather Products (ASAP) Study Report, NASA Technical Report, 65 pp. [Available from the Schwerdtfeger Library, 1225 West Dayton Street, Univ. of Wisconsin-Madison, Madison, WI 53706].

Mecikalski, J. R., and K. M. Bedka, 2005: Forecasting convective Initiation by monitoring the evolution of moving cumulus in daytime GOES imagery, *Mon. Wea. Rev.* In Press.

Miller, D., T. Ratvasky, B. Bernstein, F. McDonough, and J. W. Strapp, 1998: NASA/FAA/NCAR supercooled large droplet icing flight research: summary of winter 96-97 flight operations. Proc. 36<sup>th</sup> AIAA Aerospace Science Meeting and Exhibit, Reno, Nevada, USA.

Miller, T. P., and T. J. Casadevall, 2000: Volcanic ash hazards to aviation. *Encyclopedia of Volcanoes*, edited by H. Sigurdsson, pp. 915-930, Academic Press, San Diego, CA.

- Minnis, P., D. P. Kratz, J. A. Coakley, Jr., M. D. King, D. Garber, S. Mayor, D. F. Young, and R. Arduini, 1995: Cloud Optical Property Retrieval (Subsystem 4.3). *Clouds and the Earth's Radiant Energy System (CERES) Algorithm Theoretical Basis Document, Volume III: Cloud Analyses and Radiance Inversions (Subsystem 4)*, NASA RP 1376, Vol. 3, pp. 135-176.
- Minnis, P., D. Garber, D. Young, R. Arduini, and Y. Takano, 1998: Parameterization of reflectance and effective emittance for satellite remote sensing of cloud properties. *J. Atmos. Sci.*, **55**, 3313-3339.
- Minnis, P., W. L. Smith, Jr., D. F. Young, L. Nguyen, A. D. Rapp, P. W. Heck, S. Sun-Mack, Q. Trepte, and Y. Chen, 2001: A near real time method for deriving cloud and radiation properties from satellites for weather and climate studies. *Proc. AMS 11th Conf. Satellite Meteorology and Oceanography*, Madison, Wisconsin, Oct. 15-18, pp. 477-480.
- Moody, J. L., A. J. Wimmers, and J. C. Davenport, 1999: Remotely sensed specific humidity: Development of a derived product from the GOES Imager channel 3. *Geophys. Res. Lett.*, **26**(1), 59-62.
- Mueller, C., T. Saxen, R. Roberts, J. Wilson, T. Betancourt, S. Dettling, N. Oien, and J. Yee, 2003: NCAR Auto-Nowcast System. *Wea. Forecasting*. **18**, 545-561.
- Murray, J. J., 2002: Aviation weather applications of Earth Science Enterprise data. *Earth Observing Magazine*, **11**, No. 8, pp. 26-30.
- Nair, U. S., R. C. Weger, K. S. Kuo, and R. M. Welch, 1998: Clustering, randomness, and regularity in cloud fields 5. The nature of regular cumulus cloud fields. *J. Geophys. Res.*, **103**, 11363-11380.

- National Research Council, 1980: Technological and Scientific Opportunities for Improved Weather and Hydrological Services in the Coming Decade. Select Committee on the National Weather Service, National Academy Press, Washington, D.C., 87 pp.
- National Research Council, 1991: Toward a New National Weather Service: A First Report. National Weather Service Modernization Committee, National Academy Press, Washington, D.C., 67 pp.
- National Research Council, 1994: Weather for Those Who Fly. National Weather Service Modernization Committee, National Academy Press, Washington, D.C., 100 pp.
- Pack, D. W., C. J. Rice, B. J. Tressel, C. J. Lee-Wagner, and E. M. Oshika, 2000: Civilian uses of surveillance satellites. *Crosslink Magazine*, The Aerospace Corporation, Los Angeles, CA, 1, 2-8. [available at <http://www.aero.org/publications/crosslink/pdfs/V1N1.pdf>]
- Pavolonis, M. J., W. F. Feltz, A. K. Heidinger, and G. M. Gallina, 2005: A daytime complement to the reverse absorption technique for improved automated detection of volcanic ash. *J. Atmos. Oceanic Tech.*, Submitted.
- Platnick, S., M. D. King, S. A. Ackerman, W. P. Menzel, B. A. Baum, J. C. Riedi, R. A. Frey, 2003: The MODIS cloud products: Algorithms and examples from Terra. *IEE Trans. On Geosci. Rem. Sens.*, **41**, 459-473.
- Prata, A. J., 1989: Observations of volcanic ash clouds in the 10–12 micrometer window using AVHRR/2 data. *Int. J. Rem. Sen.*, **10**, 751-761.
- Rauber, R.M. and A. Tokay, 1991: An explanation for the existence of supercooled water at the top of cold clouds. *J. Atmos. Sci.*, **45**, 1005-1023.
- Roberts, R. D., and S. Rutledge, 2003: Nowcasting storm initiation and growth using GOES-8 and WSR-88D data. *Wea. Forecasting*, **18**, 562-584.

- Romero, R., 2004: The international airways volcano watch (IAVW). *Proceedings of the 2<sup>nd</sup> International Conference on Volcanic Ash and Aviation Safety*, Office of the Federal Coordinator for Meteorological Services and Supporting Research, Washington, D.C., Session 4, 1-10.
- Schmit, T. J., M. M. Gunshor, W. P. Menzel, J. J. Gurka, J. Li, and A. S. Bachmeier, 2005: Introducing the next-generation advanced baseline imager on GOES-R. *Bull. Amer. Meteor. Soc.*, **86**, 1079-1096.
- Schreiner, A. J., D. A. Unger, W. P. Menzel, G. P. Ellrod, K. I. Strabala, and J. L. Pellett, 1993: A comparison of ground and satellite observations of cloud cover. *Bull. Amer. Meteor. Soc.*, **74**, 1851-1861.
- Schreiner, A. J. and T. J. Schmit, 2001: Derived cloud products from the GOES-M imager. Preprints, *11<sup>th</sup> Conference on Satellite Meteorology and Oceanography*, Madison, WI, American Meteorological Society, Boston, 420-423.
- Schreiner, A. J., T. J. Schmit, and W. P. Menzel, 2001: Observations and trends of clouds based on GOES sounder data. *J. Geophys. Res.*, **106**, 20349-20363.
- Seftor, C. J., N. C. Hsu, J. R. Herman, P. K. Bhartia, O. Torres, W. I. Rose, D. J. Schneider, and N. Krotkov, 1997: Detection of volcanic ash clouds from Nimbus-7/TOMS. *J. Geophys. Res.*, **102**, 16749-16760.
- Shapiro, M. A., 1980: Turbulent mixing within tropopause folds as a mechanism for the exchange of chemical constituents between the stratosphere and troposphere. *J. Atmos. Sci.*, **37**, 994-1004.

- Trepte, Q., Y. Chen, S. Sun-Mack, P. Minnis, D. Young, B. Baum, and P. Heck, 1999: Scene identification for the CERES cloud analysis subsystem. *Proc. AMS 10<sup>th</sup> Conf. Atmos. Rad.*, Madison, Wisconsin, 28 June – 2 July, pp. 169-172.
- Triplett, William, 2005: The Calculators of Calm. Air & Space Smithsonian, pp. 54-61.
- Velden, C. S., C. M. Hayden, S. J. Nieman, W. P. Menzel, S. Wanzong, and J. S. Goerss, 1997: Upper-tropospheric winds derived from geostationary satellite water vapor observations. *Bull. Amer. Meteor. Soc.*, **78**, 173-195.
- Velden, T. L. Olander, and S. Wanzong, 1998: The impact of multispectral GOES-8 wind information on Atlantic tropical cyclone track forecasts in 1995. Part I: Dataset methodology, description, and case analysis. *Mon. Wea. Rev.*, **126**, 1202-1218.
- Velden, C.S., J. Daniels, D. Stettner, J. Dunion, D. Santek, J. Key, J. Dunion, K. Holmlund, G. Dengel, W. Bresky, and P. Menzel, 2005: Recent innovations in deriving tropospheric winds from meteorological satellites. *Bull. Amer. Meteor. Soc.*, **86**, 205-223.
- Vivekanandan, J., G. Thompson, and T. Lee, 1996: Aircraft icing detection using satellite data and weather forecast model results. *Proc. FAA Intl. Conf. On Aircraft Icing*, Springfield, Virginia, May 6-8, 1996.
- Wimmers, A. J., and J. L. Moody 2001: A fixed-layer estimation of upper tropospheric specific humidity from the GOES water vapor channel: Parameterization and validation of the altered brightness temperature product. *J. Geophys. Res.*, **106** (D15), 17115-17132.
- Wimmers, A. J., and J. L. Moody, 2004a: Tropopause folding at satellite-observed spatial gradients. I. Verification of an empirical relationship. *J. Geophys. Res.*, **109** D19306, doi:10.1029/2003JD004145.

Wimmers, A. J., and J. L. Moody, 2004b: Tropopause folding at satellite-observed spatial gradients. II. Development of an empirical model. *J. Geophys. Res.*, **109**, D19307, doi:10.1029/2003JD004146.

Wolff, C., B. Bernstein, and F. McDonough, 2005: Nowcasting aircraft icing conditions using GOES-derived satellite products. *WWRO Symposium on Nowcasting and Very Short Range Forecasting*, Toulouse, France, 5-9 September.

Wylie, D. P., and W. P. Menzel, 1989: Two years of cloud cover statistics using VAS. *J. Climate*, **2**, 380-392.

**List of Figures:**

**Figure 1:** Example of the GOES-12 Imager derived cloud top pressure product from 15 November 2005 at 1800 UTC.

**Figure 2:** GOES-12 Sounder (blue), GOES-12 Imager (red) and CPL (black) derived cloud top height for the entire flight of the NASA ER-2 on 05 December 2003.

**Figure 3:** Histogram of the absolute differences between the CPL and GOES-12 Sounder (blue) and Imager (red) cloud top height for 05 December 2003.

**Figure 4:** Texture-based clustering of GOES imagery. Three band RGB image is shown in A) while the color-coded clustering classifier results are shown in B).

**Figure 5:** (top panels) AMVs (in knots) within the 100-70, 70-40, and 40-10 kPa layers, respectively, constrained to the NWP background wind field at 2000 UTC on 4 May 2003. (bottom panels) AMVs within the same atmospheric layers, using the Bedka and Mecikalski (2005) technique, where the background wind field is down-weighted, allowing for the depiction of synoptic- and meso-scale flow.

**Figure 6:** An example of the 30-minute cloud-top cooling rate (upper-right) calculated using the techniques described in Bedka and Mecikalski (2005) at 2000 UTC on 4 May 2003. Developing convection is outlined with ovals within the GOES-12 10.7  $\mu\text{m}$  brightness temperature imagery

at 1930 UTC (upper-left) and 2000 UTC (lower-left). The mean 30-minute cooling rate, identified by a human expert, is displayed in the upper-left.

**Figure 7:** The CI nowcast product at 2000 UTC on 4 May 2003. Pixels highlighted in red have met at least seven of the eight CI criteria and need to be monitored for future CI over the following 30-45 minutes. Grey pixels represent mature cumulus and cirrus identified classified by the ASAP convective cloud mask.

**Figure 8:** GOES-derived cloud-top cooling rates as used with the NCAR Auto-Nowcast system. Data developed from the Mecikalski and Bedka (2005) algorithm using atmospheric motion vectors as described by Bedka and Mecikalski (2005).

**Figure 9:** Cloud liquid water path (a) and effective radius (b) as derived by the NASA LaRC VISST algorithm on 19 January 2005 at 1915 UTC.

**Figure 10:** Mountain wave automated identification in MODIS imagery at 0517 UTC 25 June 2003 over southern Colorado. Laplacian of Gaussian (LoG) Zero crossing applied to contrast enhanced MODIS 6.7  $\mu\text{m}$  water vapor imagery. Bright pixels in LoG zero crossing image correspond to a strong change in gradient direction and magnitude, indicating possible turbulence.

**Figure 11:** Sample CAT-prediction model. Base image, GLASH (GOES Layer Average Specific Humidity), derived from the GOES water vapor channel (the red-yellow colors are subtropical

air and the blue-purple colors are dry polar air); Grey regions are estimated areas of tropopause folding, extending toward and underneath the side of the warmer air mass; red disks are pilot reports of turbulence inside the volume of the predicted tropopause fold (the corresponding key is in the corner of the image); the numbers beside the pilot reports indicate the potential temperature difference between the pilot report and the central potential temperature of the fold.

**Figure 12:** True color Aqua-MODIS images capturing an eruption of Manam on October 24, 2004, 0355 UTC. The top image is an unaltered true color image of the scene, the results of the new multispectral volcanic ash mask are overlaid on the middle image, and the ash mask given by identifying pixels with an 11—12  $\mu\text{m}$  brightness temperature difference less than 0.0 (reverse absorption technique) is shown in the bottom image. The new algorithm clearly improves upon the standard reverse absorption technique and also provides information on the location of ice clouds that are contaminated with volcanic aerosols.

**Figure 13:** Clustering results using MODIS imagery of the Manam volcano. Volcanic ash cluster are shown as red in the lower right image.

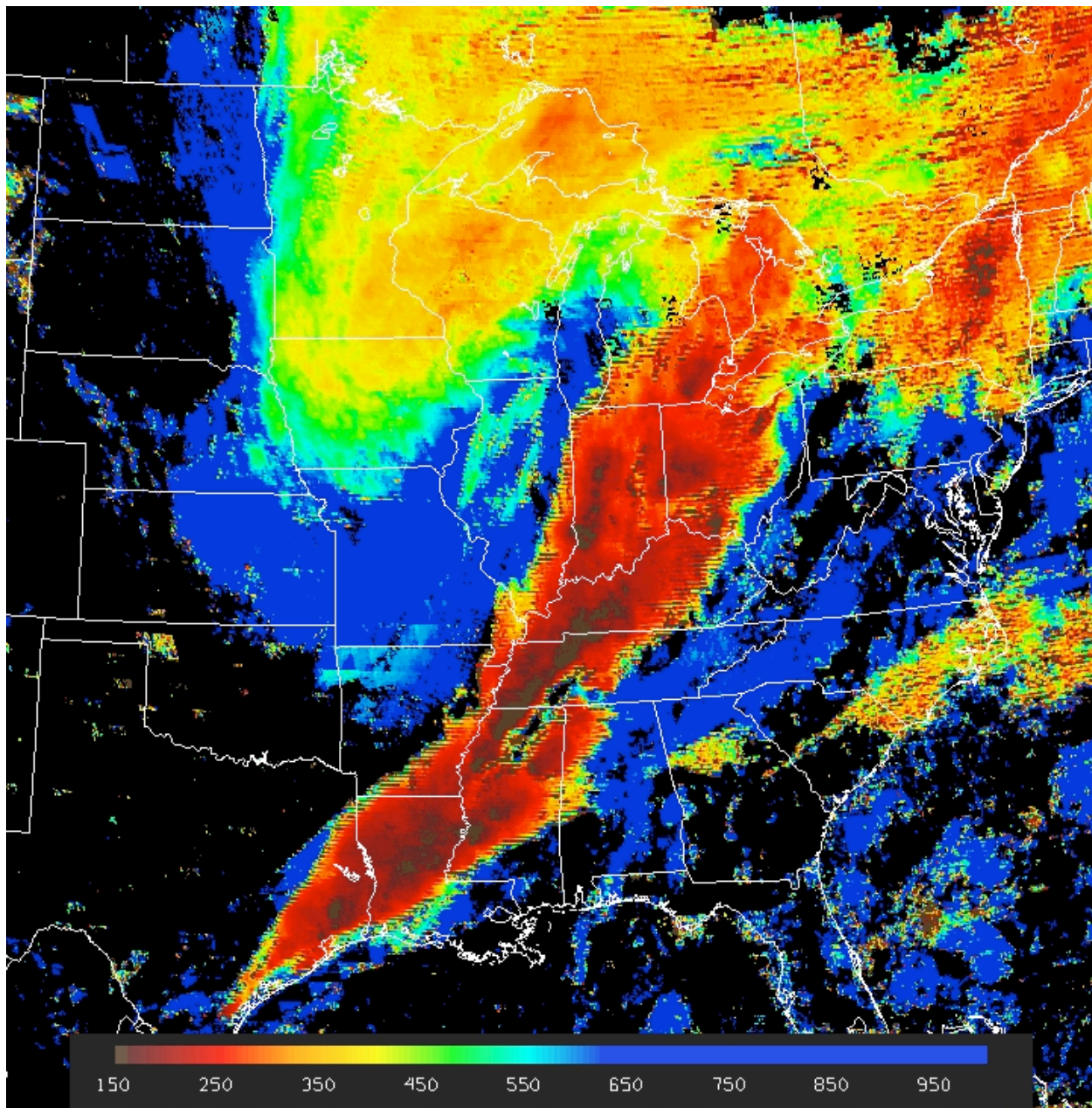


**Figure 1:** Example of the GOES-12 Imager derived cloud top pressure product from 15 November 2005 at 1800 UTC.

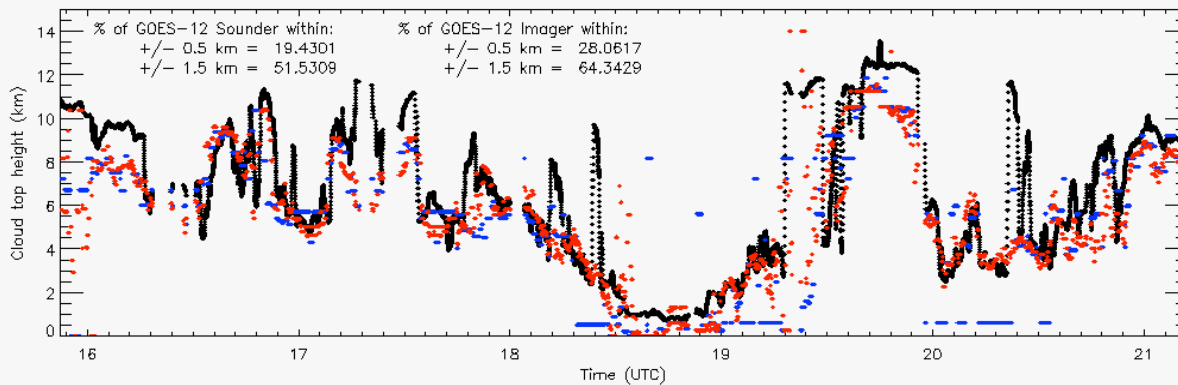


**Figure 2:** GOES-12 Sounder (blue), GOES-12 Imager (red) and CPL (black) derived cloud top height for the entire flight of the NASA ER-2 on 05 December 2003.

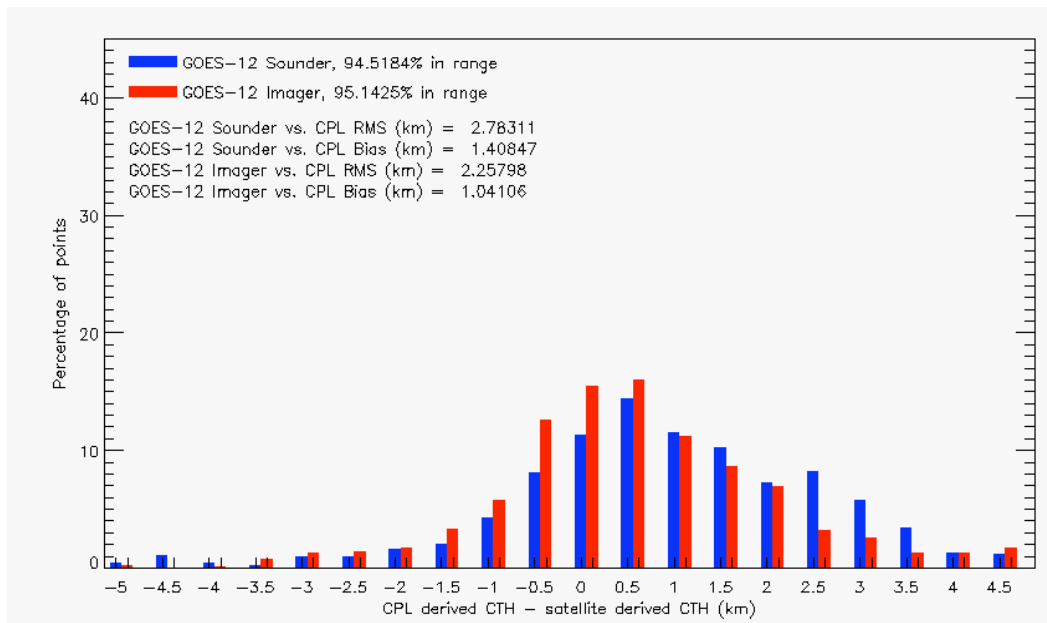


**Figure 3:** Histogram of the absolute differences between the CPL and GOES-12 Sounder (blue) and Imager (red) cloud top height for 05 December 2003.

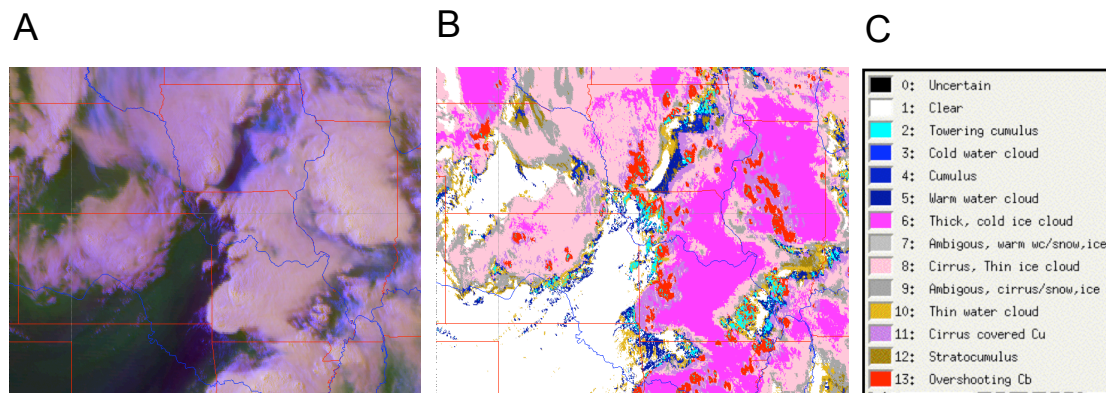


**Figure 4:** Texture-based clustering of GOES imagery. Three band RGB image is shown in A), the color-coded clustering classifier results are shown in B), and the legend is shown in C).

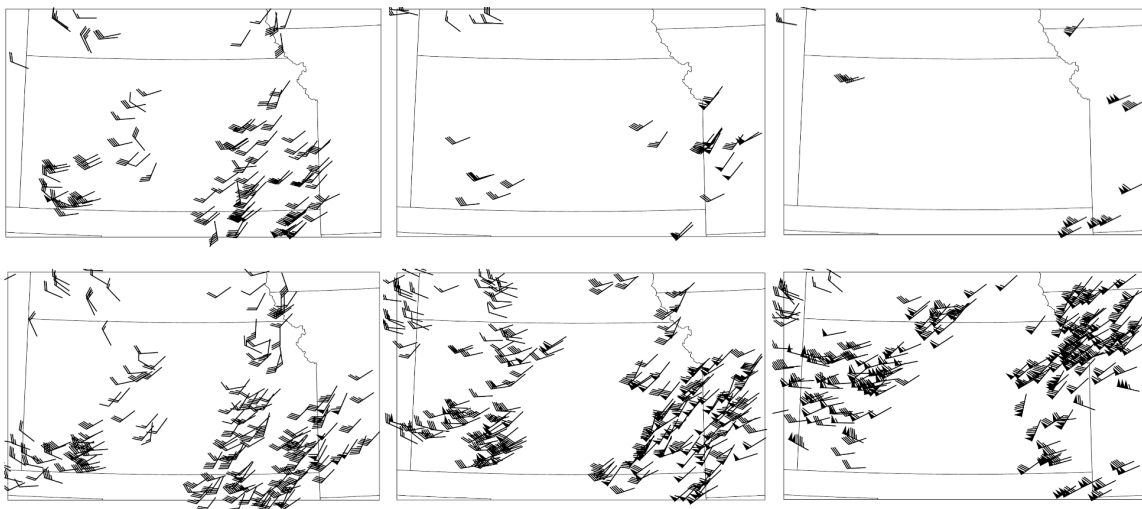


**Figure 5:** (top panels) AMVs (in knots) within the 100-70, 70-40, and 40-10 kPa layers, respectively, constrained to the NWP background wind field at 2000 UTC on 4 May 2003. (bottom panels) AMVs within the same atmospheric layers, using the Bedka and Mecikalski (2005) technique, where the background wind field is down-weighted, allowing for the depiction of synoptic- and meso-scale flow. Only 20% of the total AMVs in the bottom panels are randomly selected for display clarity.

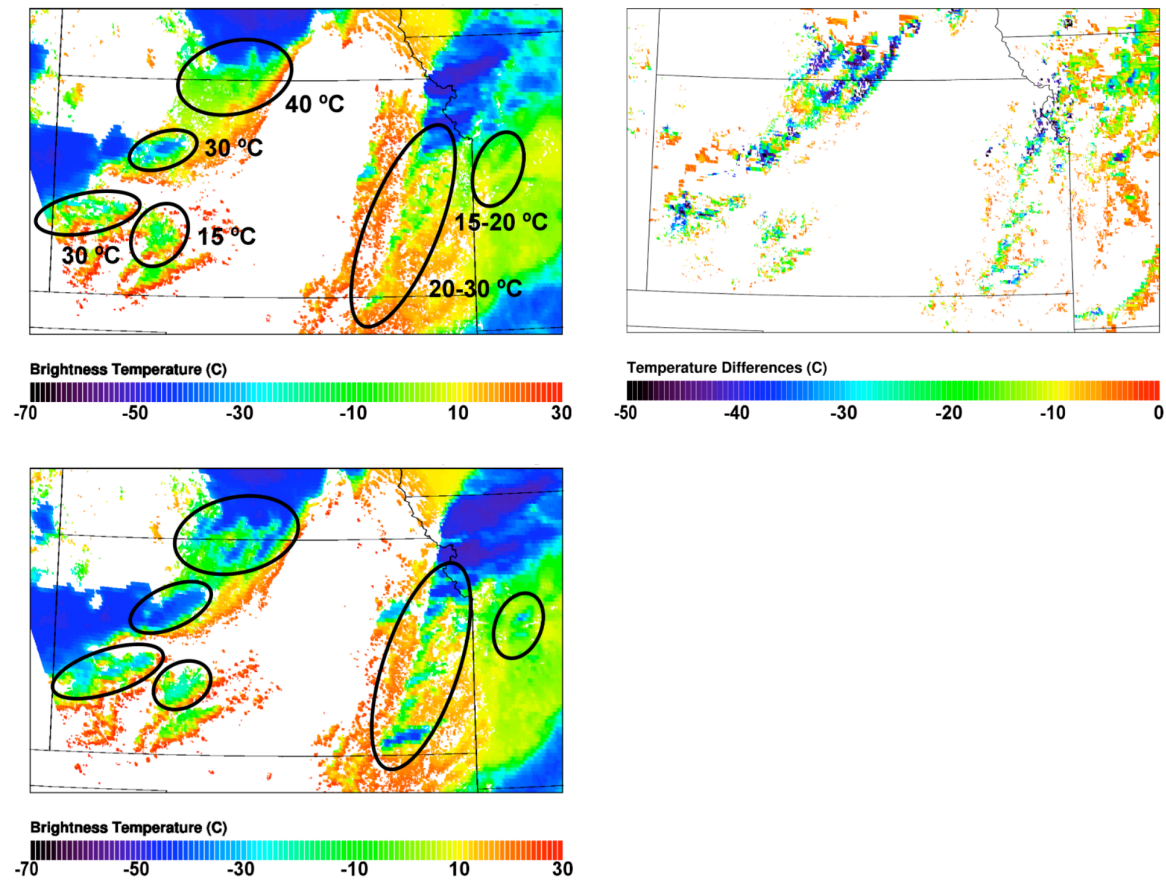


**Figure 6:** An example of the 30-minute cloud-top cooling rate (upper-right) calculated using the techniques described in Bedka and Mecikalski (2005) at 2000 UTC on 4 May 2003. Developing convection is outlined with ovals within the GOES-12 10.7  $\mu\text{m}$  brightness temperature imagery at 1930 UTC (upper-left) and 2000 UTC (lower-left). The mean 30-minute cooling rate, identified by a human expert, is displayed in the upper-left.

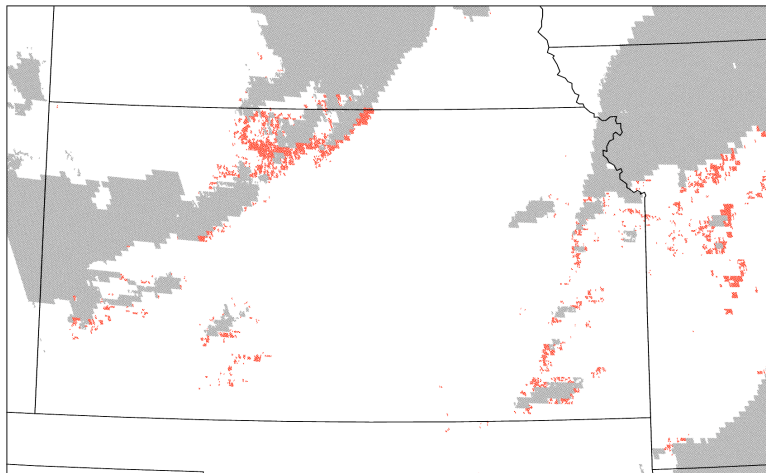


**Figure 7:** The CI nowcast product at 2000 UTC on 4 May 2003. Pixels highlighted in red have met at least seven of the eight CI criteria and need to be monitored for future CI over the following 30-45 minutes. Grey pixels represent mature cumulus and cirrus identified classified by the ASAP convective cloud mask.

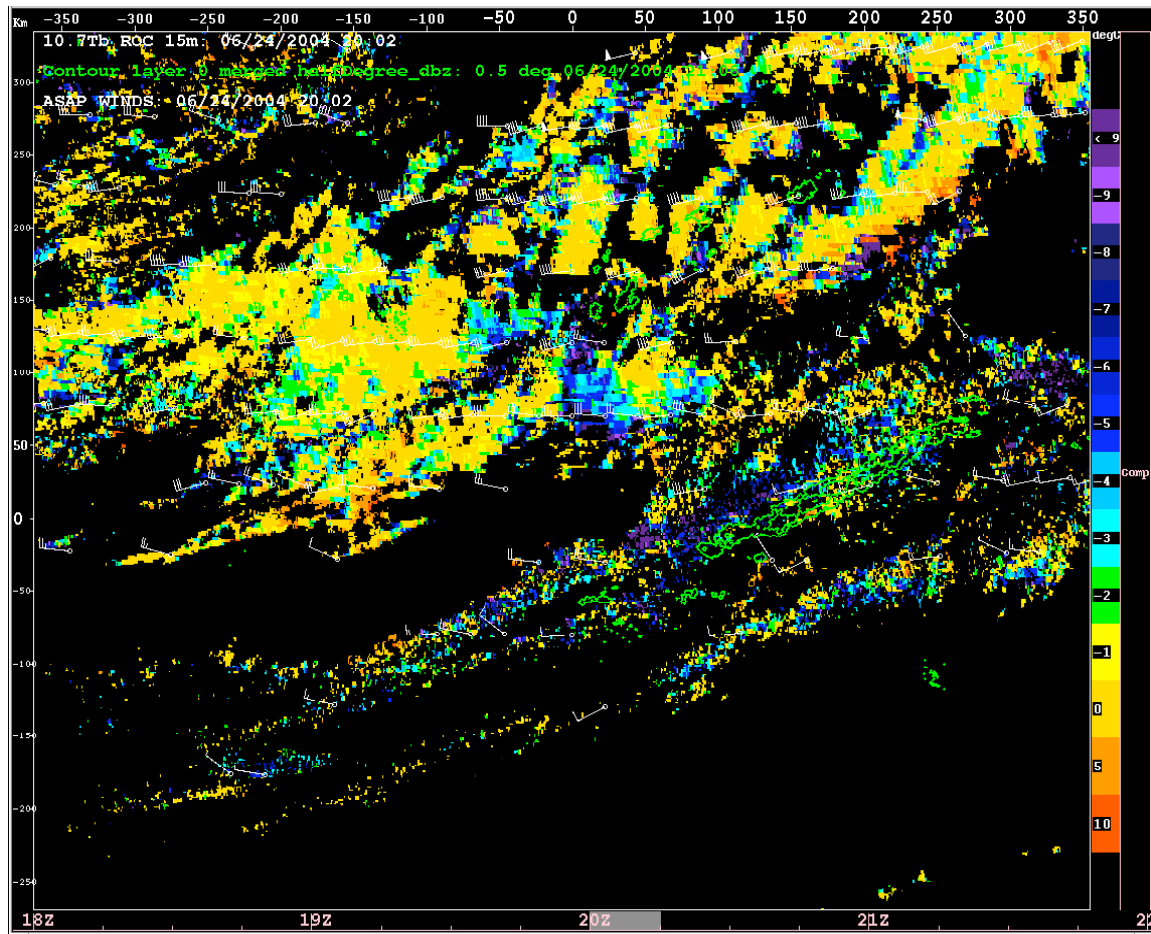
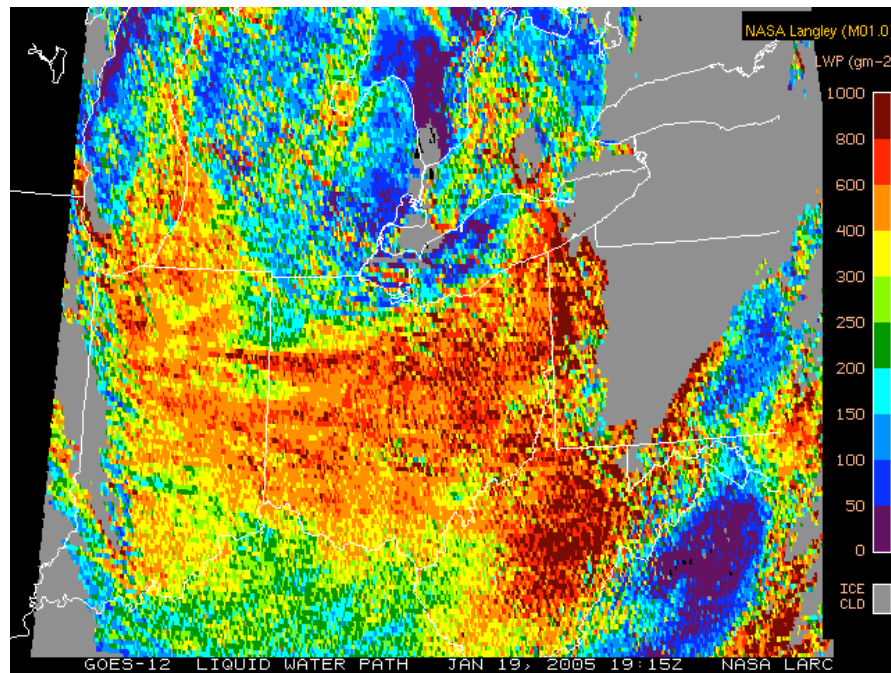
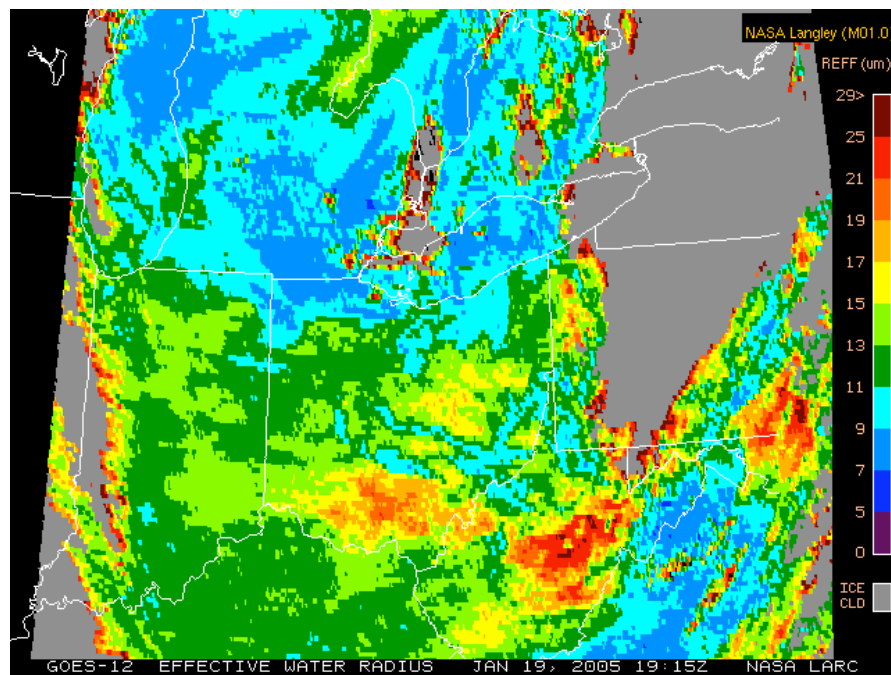


**Figure 8:** GOES-derived cloud-top cooling rates as used with the NCAR Auto-Nowcast system.



(a)



(b)

**Figure 9:** Cloud liquid water path (a) and effective radius (b) as derived by the NASA LaRC VISST algorithm on 19 January 2005 at 1915 UTC.

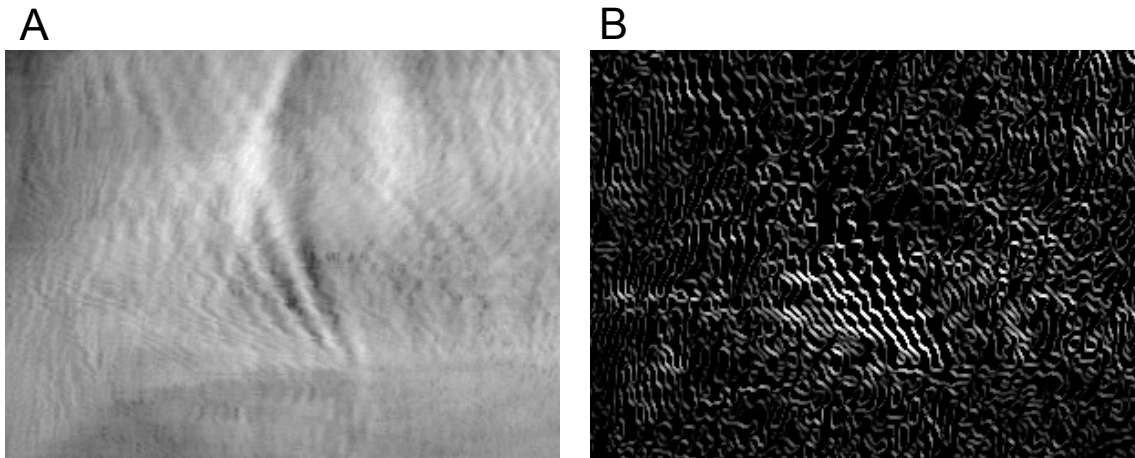


**Figure 10:** Mountain wave automated identification in MODIS imagery at 0517 UTC 25 June 2003 over southern Colorado. Laplacian of Gaussian (LoG) Zero crossing applied to contrast enhanced MODIS 6.7  $\mu\text{m}$  water vapor imagery. Bright pixels in LoG zero crossing image correspond to a strong change in gradient direction and magnitude, indicating possible turbulence.

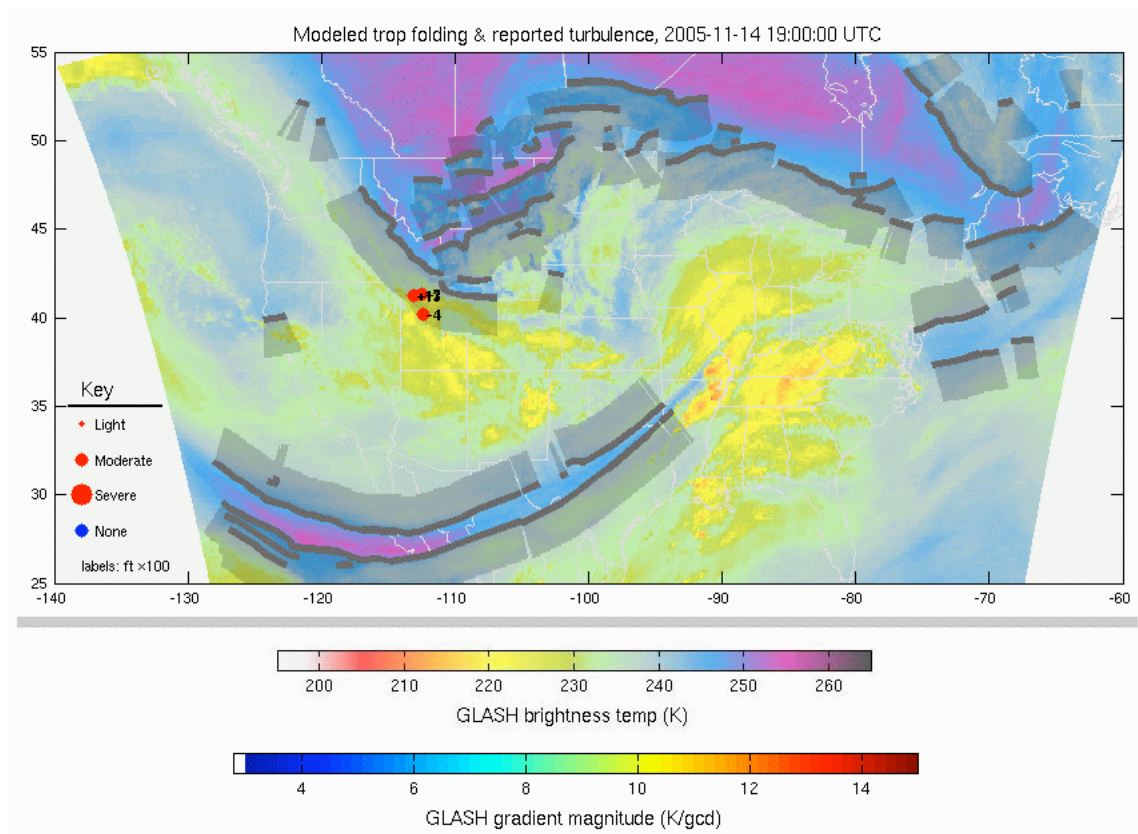


**Figure 11:** Sample CAT-prediction model. Base image, GLASH (GOES Layer Average Specific Humidity), derived from the GOES water vapor channel (the red-yellow colors are subtropical air and the blue-purple colors are dry polar air); Grey regions are estimated areas of tropopause folding, extending toward and underneath the side of the warmer air mass; red disks are pilot reports of turbulence inside the volume of the predicted tropopause fold (the corresponding key is in the corner of the image); the numbers beside the pilot reports indicate the potential temperature difference between the pilot report and the central potential temperature of the fold.

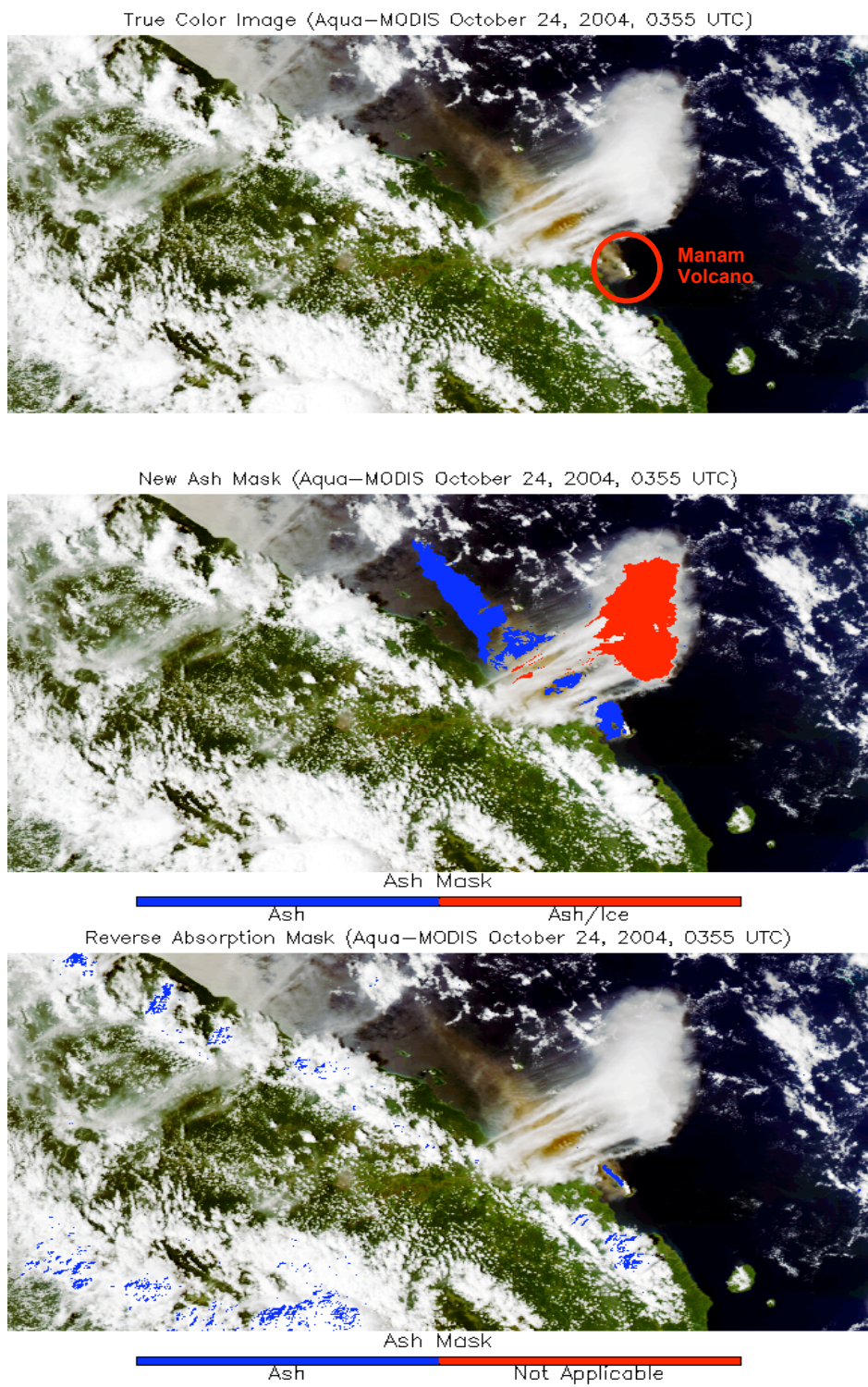


**Figure 12:** True color Aqua-MODIS images capturing an eruption of Manam on October 24, 2004, 0355 UTC. The top image is an unaltered true color image of the scene, the results of the new multispectral volcanic ash mask are overlaid on the middle image, and the ash mask given by identifying pixels with an 11–12  $\mu\text{m}$  brightness temperature difference less than 0.0 (reverse absorption technique) is shown in the bottom image.

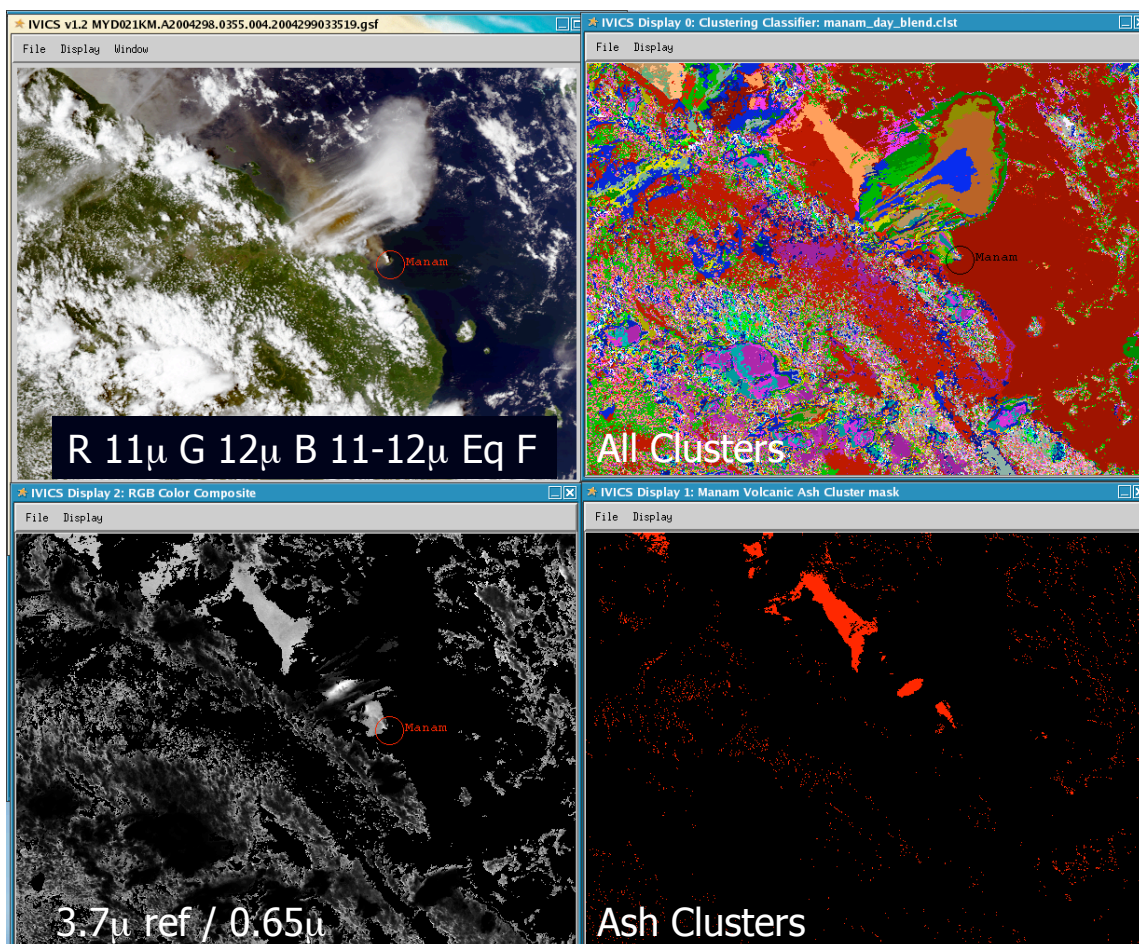


**Figure 13:** Clustering results using MODIS imagery of the Manam volcano. Volcanic ash cluster are shown as red in the lower right image.